

This is a repository copy of *Fast quantitative elemental mapping of highly inhomogeneous materials by micro-Laser-Induced Breakdown Spectroscopy*.

White Rose Research Online URL for this paper:

<https://eprints.whiterose.ac.uk/130416/>

Version: Accepted Version

---

**Article:**

Pagnotta, Stefano, Lezzerini, Marco, Campanella, Beatrice et al. (8 more authors) (2018) Fast quantitative elemental mapping of highly inhomogeneous materials by micro-Laser-Induced Breakdown Spectroscopy. *Spectrochimica Acta Part B: Atomic Spectroscopy*. 9–15. ISSN 0584-8547

<https://doi.org/10.1016/j.sab.2018.04.018>

---

**Reuse**

This article is distributed under the terms of the Creative Commons Attribution-NonCommercial-NoDerivs (CC BY-NC-ND) licence. This licence only allows you to download this work and share it with others as long as you credit the authors, but you can't change the article in any way or use it commercially. More information and the full terms of the licence here: <https://creativecommons.org/licenses/>

**Takedown**

If you consider content in White Rose Research Online to be in breach of UK law, please notify us by emailing [eprints@whiterose.ac.uk](mailto:eprints@whiterose.ac.uk) including the URL of the record and the reason for the withdrawal request.

1 Fast quantitative elemental mapping of highly inhomogeneous materials by  
2 micro-Laser-Induced Breakdown Spectroscopy  
3

4 S. Pagnotta<sup>a,b\*</sup>, M. Lezzerini<sup>b</sup>, B. Campanella<sup>a</sup>, G. Gallelo<sup>d</sup>, E. Grifoni<sup>a</sup>, S. Legnaioli<sup>a</sup>, G.  
5 Lorenzetti<sup>a</sup>, F. Poggialini<sup>a</sup>, S. Raneri<sup>b</sup>, A. Safi<sup>c</sup>, V. Palleschi<sup>a</sup>

6 <sup>a</sup> Applied and Laser Spectroscopy Laboratory, Institute of Chemistry of Organometallic Compounds,  
7 Research Area of National Research Council, Via G. Moruzzi, 1 – 56124 Pisa, Italy

8 <sup>b</sup>Department of Earth Sciences, University of Pisa, Via Santa Maria 53, Pisa, Italy

9 <sup>c</sup>Laser and Plasma Research Institute, Shahid Beheshti University, G. C., Evin, Tehran, 1983963113  
10 Iran

11 <sup>d</sup>Department of Archaeology, University of York, King's Manor, YO17EP York, UK  
12  
13  
14

15 **Abstract**  
16

17 In this work, a fast method for obtaining a quantitative elemental mapping of highly inhomogeneous  
18 samples by  $\mu$ -LIBS maps is proposed. The method, transportable and cheap, allows the analysis of  
19 large maps through the use of a Self-Organizing Map clustering method coupled to Calibration-Free  
20 LIBS for quantification of cluster prototypes. The method proposed has been verified on  
21 heterogeneous materials such historical lime mortars but it can be easily applied to a larger class of  
22 inhomogeneous materials for very different applications (modern building materials, biological  
23 samples, industrial materials, etc.).  
24  
25  
26  
27  
28  
29  
30

31 **Keywords:** LIBS, Elemental Mapping, Calibration-Free LIBS, Self-Organizing Maps, Mortars  
32  
33

34 \* *Corresponding author:* stefanopagnotta@yahoo.it

35 **1. Introduction**

36

37 Laser-based techniques have attracted a considerable interest in the last decades for their capability  
38 of obtaining elemental images of solid samples without specific treatment, with high spatial resolution  
39 and at different depths [1-5]. A number of applications have been proposed in several fields, ranging  
40 from biomedical, geological and environmental research, to forensic analysis, to industrial  
41 diagnostics, to Cultural Heritage study and conservation [6-13].

42 Among these techniques, applications based on the  $\mu$ -LIBS technique are becoming more and more  
43 frequent to scan surfaces and obtain compositional maps, providing interesting results in a number of  
44 applications that require qualitative and quantitative analyses [14-22]. The use of  $\mu$ -LIBS-scan  
45 technique has proved to be very advantageous from an economic and experimental point of view with  
46 respect to other laser-based techniques such as Laser-Ablation-Inductively Coupled Plasma-Mass  
47 Spectrometry (LA-ICP-MS) [23]. The method is, in fact, fast, transportable, relatively cheap and can  
48 analyse simultaneously elements with very different ionization energy, a task that can be problematic  
49 in LA-ICP-MS [24]. While the qualitative analysis of  $\mu$ -LIBS elemental maps is a relatively simple  
50 task, the quantification of the elemental composition of the sample is much more challenging. In  
51 principle, a quantitative analysis based on the use of reference samples of known composition for  
52 building linear or non-linear, uni- or multi-variate calibration surfaces is applicable only when the  
53 matrix of the sample remains more or less constant in the region of analysis [25]. If the sample is  
54 characterized by strong inhomogeneities, with materials of different matrixes, or when suitable  
55 reference samples are not available, a possible approach to quantitative elemental mapping would be  
56 the use of Calibration-Free approaches [25-27]. An important drawback of the CF-LIBS approach,  
57 however, is the time required for the analysis: **the emission lines of the elements in the samples must  
58 be individuated and their intensities calculated through their fit with a Voigt profile. The electron  
59 number density must be calculated from the Stark broadening of the hydrogen Balmer alpha line, then  
60 the electron temperature must be calculated from the Boltzmann or Saha-Boltzmann plot. Finally, the  
61 sample composition must be calculated. If automated all these operations take at least less than 30  
62 seconds per spectrum; however,  $\mu$ -LIBS elemental maps with megapixel spatial resolution have been  
63 obtained by different groups, and a CF-LIBS approach applied on millions of LIBS spectra is, at the  
64 moment, unrealistic. D'Andrea et al. [28] have recently proposed a hybrid Artificial Neural Network  
65 (ANN) – CF-LIBS method that can be very effective in most of the cases, but requires the variations  
66 in the material matrix to be relatively small for the ANN to work properly.**

67 In this work, we propose a method based on the sequential application of elemental map segmentation  
68 (obtained using an automatic classification method based on the use of Self-Organizing Maps, as

69 proposed by the authors in [29]), followed by a CF-LIBS analysis of the prototypal spectra  
70 representing the different clusters (materials) in the map. The method is presented and tested for the  
71 analysis of ancient mortars. The knowledge developed in the study of this class of highly  
72 inhomogeneous materials may have also interesting applications in the analysis and study of modern  
73 binding materials and techniques.

74

## 75 **2. Materials and methods**

76

77 To assess the analytical capability of the method proposed, two mortar fragments from the Norman  
78 Adrano Castle (Catania, Sicily) were selected as test samples. The two samples (labelled with the  
79 inventory numbers N2-2 and S2-3) have been analysed with the permission of the *Soprintendenza*  
80 *per i Beni culturali e Ambientali di Catania*. They consist of polished thin sections consolidated by  
81 epoxy resin; the mortars are characterized by a heterogeneous binder with the presence of aggregates  
82 due to volcanic ash, with a large variation in grain size (figure 1).

83 The analysis of ancient mortars is one of the main topics of Earth Sciences disciplines applied to  
84 Cultural Heritages. Usually, ancient mortars are classified in two main categories, lime-aerial mortars  
85 and hydraulic lime mortars. The latter ones were often obtained by adding to the mixtures volcanic  
86 materials ("pozzolana"), and crushed ceramic fragments ("cocciopesto"). In both cases, the final  
87 product is a mixture characterised by a relatively homogeneous paste, embedding inside clasts of  
88 various dimension. The ability of pozzolanic materials to provide hydraulic proprieties to the mortars  
89 is due to the presence of reactive constituents like aluminates and silicates [30]. A quantitative  
90 elemental mapping could thus give information about the typology of analyzed mortars (aerial vs.  
91 hydraulic) and well as the degree of hydraulicity (Vicat formula [31]). Usually, the characterization  
92 of ancient mortars is achieved by optical microscopy (OM), X-ray fluorescence (XRF), X-ray  
93 diffraction (XRD), scanning electron microscope (SEM-EDS), termogravimetric methods [32] and  
94 inductively coupled plasma mass spectrometry (ICP-MS) [33]. However, from an analytical point of  
95 view, the heterogeneity proper of these kind of materials and the presence of low crystalline CSH  
96 (Calcium-Silicate-Hydrated) phases [34,35] represent, sometimes, a limit for the complete  
97 characterization of mortars, especially considering the difficult to delineate the spatial distribution  
98 and the occurrence of CSH with respect to binder and aggregates.

99 An interesting method based on semi-automated algorithm working on elementary maps obtained by  
100 SEM-EDS data has recently been proposed by Belfiore et al. [36].



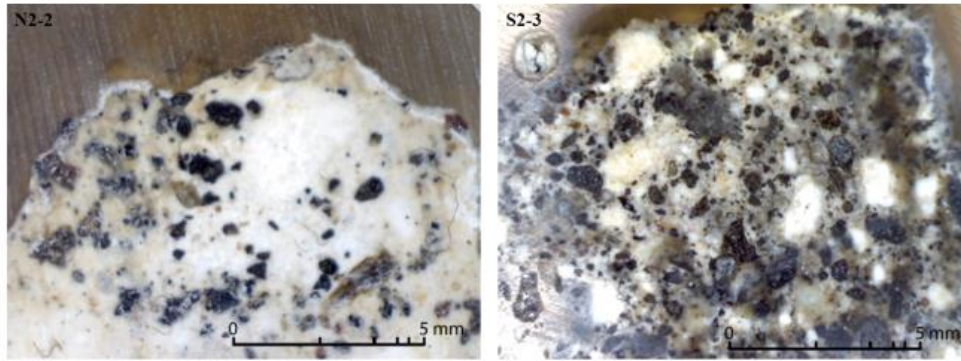


Figure 1. Microphotography of the two mortar samples.

101

102

103

### 104 3. Experimental procedure

105

106 A  $\mu$ -Modi double-pulse instrument [37], equipped with a collinear double-pulse Nd:YAG Laser  
 107 ( $\lambda=1064$  nm) coupled with a Zeiss Axio Plan A1 microscope with 10X objective was used for the  
 108 mapping of the samples. The energy of the two pulses was set to 20 mJ and 30 mJ, respectively, in  
 109 20 ns FWHM [38]. The delay between the laser pulses was set at 1 $\mu$ s. The LIBS signal was collected  
 110 using an optical fiber, placed at 45 $^\circ$  with respect to the laser direction, at a distance of about 1 cm  
 111 from the sample. A ball lens in front of the fiber guarantees the optimal collection of the LIBS signal  
 112 from the whole plasma. The  $\mu$ -Modi instrument uses an Avantes double spectrometer (AvaSpec-  
 113 2048-2), covering the spectral region from 190 to 900 nm (0.1 nm resolution from 190 to 450 nm, 0.3  
 114 nm resolution from 450 to 900 nm). The spectra were acquired 250 ns after the second laser pulse.  
 115 The acquisition time of the spectrometer is of about 2 ms (time-integrated measurements). The  
 116 samples were placed on a motorized X-Y sample holder, synchronized with the laser and spectrometer  
 117 through a LabVIEW $^\circledR$  dedicated software. The element maps were acquired on a 50x50 matrix (2500  
 118 LIBS spectra) with a lateral resolution of 100  $\mu$ m, for a total scanned area of 25 mm $^2$ , **with the laser**  
 119 **operating at 1 Hz repetition rate**. The diameter of the laser crater at the sample surface was about 20  
 120  $\mu$ m [29].

121 The main elements present in the mortars are reported in **table I**, along with the central wavelength of  
 122 the emission line used for building the compositional images from the LIBS spectra. Given the  
 123 qualitative nature of the analysis, at this stage, the use of self-absorbed resonant lines is tolerable.

124

125

126 Table I - Selected elements and central wavelength of the line considered

Element	Ion.	$\lambda(\text{nm})$
C	I	247.8
Na	I	589.0
Mg	II	279.4
Al	I	309.3
Si	I	288.2
Fe	I	372.0
Ca	I	445.2

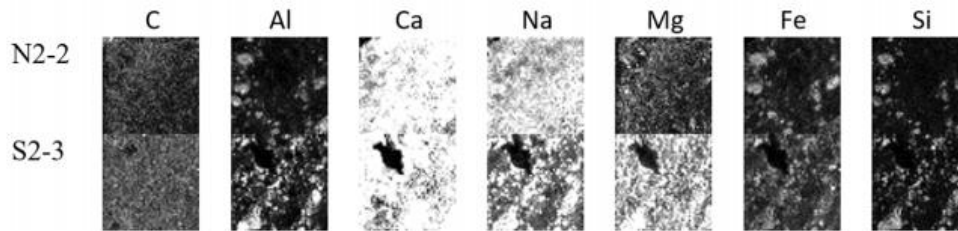
127  
128

129 **4. Results**

130

131 Based on the intensity of the lines identified, a series of elementary maps constituting the starting  
132 point for the subsequent clusterization (or segmentation) processing were obtained, as shown in **figure**  
133 **2**.

134



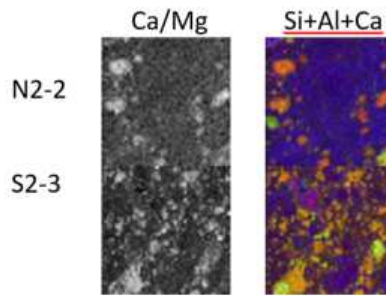
135

136 Figure 2. The elemental maps obtained by  $\mu$ -LIBS scan

137

138 Following the method described in ref. [29], for the qualitative characterization of the spatial  
139 relationship between aggregate and binder we realized for both the samples a grayscale map of the  
140 Ca/Mg line intensity ratio and a false-color map of the distribution of Si (red), Al (green) and Ca  
141 (blue) line intensity (see **figure 3**).

142 The Ca/Mg ratio maps allow us to easily discriminate the distribution of binder (dark areas) and  
143 aggregates present in mortar (bright areas). The Si-Al-Ca false-color maps evidence further the high  
144 inhomogeneity of the samples.



145

146 Figure 3. At the left, the map representing the Ca/Mg line intensity ratio. At the right, the false-color map  
 147 representing the distribution of Si (red), Al (green) and Ca (blue) line intensity.

148

149 Although clear from a qualitative point of view, the differences in the sample matrix from point to  
 150 point prevent the possibility of using a unique calibration strategy based on the construction of  
 151 univariate calibration curves or multivariate linear (Partial Least Square Analysis, for example) or  
 152 non-linear (Artificial Neural Networks) approaches.

153 The first step of our proposed analytical strategy is thus the automatic segmentation of the elemental  
 154 images using a Self-Organizing Map neural network [39], with the purpose of detecting and  
 155 separating the different components in the samples.

156 The SOM network is an unsupervised neural network that consists of neurons organized in a low-  
 157 dimensional network. Each neuron is represented by an n-dimensional weight vector where n is the  
 158 number of dimensions of the input vectors (in our case, n=7, corresponding to the peak intensity of  
 159 the lines reported in table I). The input vectors are normalized to have unit length. The samples (in  
 160 our case, the set of LIBS spectra defining the 'pixels' of the image) are assigned to the nodes whose  
 161 weights are 'closer' to their LIBS spectra. The different neurons adjust their weights in order to get  
 162 the largest possible number of samples, in a competitive way.

163 The use of SOM networks is suitable for detecting the topology of samples [40-41] and, at the same  
 164 time, operating in a multidimensional parameters space without reducing the dimensionality of the  
 165 system [42]. Since the number of different materials in the mortars is not known a priori, we chose a  
 166 5-neuron SOM which will select a maximum of 5 independent clusters (figure 4). These clusters  
 167 should well represent the inhomogeneity of the sample. Given the unavoidable slight experimental  
 168 differences between the two acquisitions, each sample was segmented independently on the other.

169



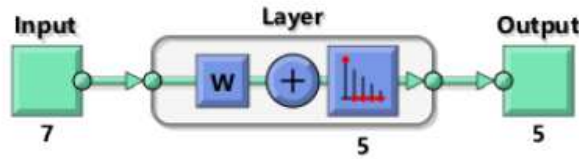


Figure 4. The network scheme: 7 inputs (peak line intensities), 5 segments as output.

170  
171  
172  
173  
174  
175  
176

Five segments for each sample was therefore obtained (figure 5). Each image obtained from SOM segmentation represents materials with similar composition/matrix [29].

	Seg. 1	Seg.2	Seg.3	Seg.4	Seg.5
N2-2					
pixel	238	309	20	744	1189
S2-3					
pixel	523	677	682	455	163

177

Figure 5. Image segmentation produced by the SOM neural network with the number of pixels represented.

178  
179

In both the mortar samples studied, the SOM segmentation reproduces similar patterns, although not corresponding to the same cluster number. For example, the regions of the samples where the epoxy resin used for consolidating the samples is exposed are clearly evidenced in segment 3 for sample N2-2 and segment 5 for sample S2-3.

184

As an interesting by-product of this classification, the area covered by each material can be estimated by the ratio between the pixel associated with a given cluster and the total number of pixels of the map. While the surface exposed in sample N2-2 is negligible (20 pixels over 2500 = 0.8 %), the corresponding exposed surface on sample S2-3 corresponds to 163 pixels over 2500 = 6.5 %.

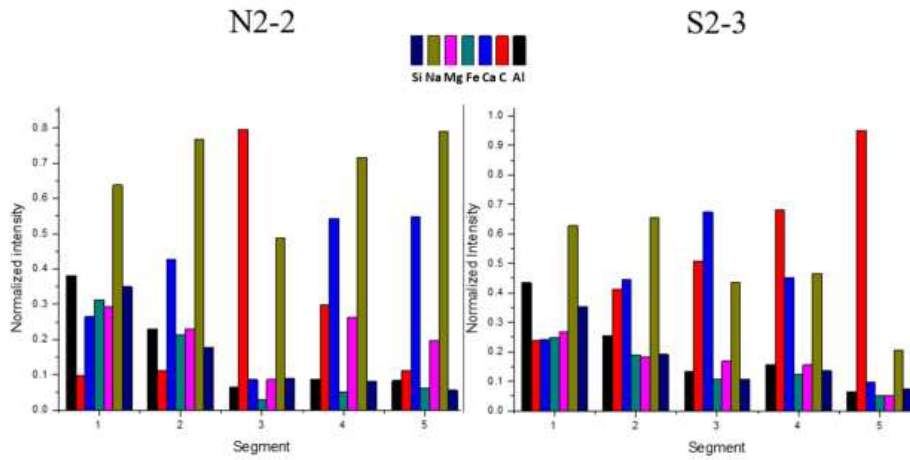
188

It is evident that averaging the LIBS spectra over the whole map would give unreliable results, that would be strongly affected by the amount of clasts, the exposed epoxy resin, etc., in the scanning area. Thus, the quantitative determination of the composition of the samples must be done separately for the different clusters/materials evidenced by the SOM classification. As discussed in [29], the SOM segmentation gives the 'coordinates' (normalized peak line intensities, since the input vectors are normalized to have unit length) of the centroids of the clusters (see figure 6). However, the centroids of the clusters do not necessarily coincide with the coordinates of a 'pixel' of the image. In

194



195 other words, the corresponding intensities does not match any physical LIBS spectrum, so this  
 196 information cannot be used for a Calibration-Free quantitative analysis.



197  
 198 Figure 6 – Normalized intensities corresponding to the centroid of the distribution.

199  
 200 On the other hand, the materials corresponding to each cluster have a homogeneous distribution  
 201 within the cluster, therefore we can average the spectra corresponding to each cluster and apply the  
 202 CF-LIBS method to these spectra only, obtaining the quantitative composition of the materials in the  
 203 sample.

204 The emission lines considered for the quantitative analysis are reported, with the corresponding  
 205 spectral parameters, in table II. The lines were chosen trying to avoid strong self-absorbed emissions,  
 206 whenever possible.

207  
 208 Table II - Emission lines used for the CF-LIBS analysis and their relevant spectral parameters

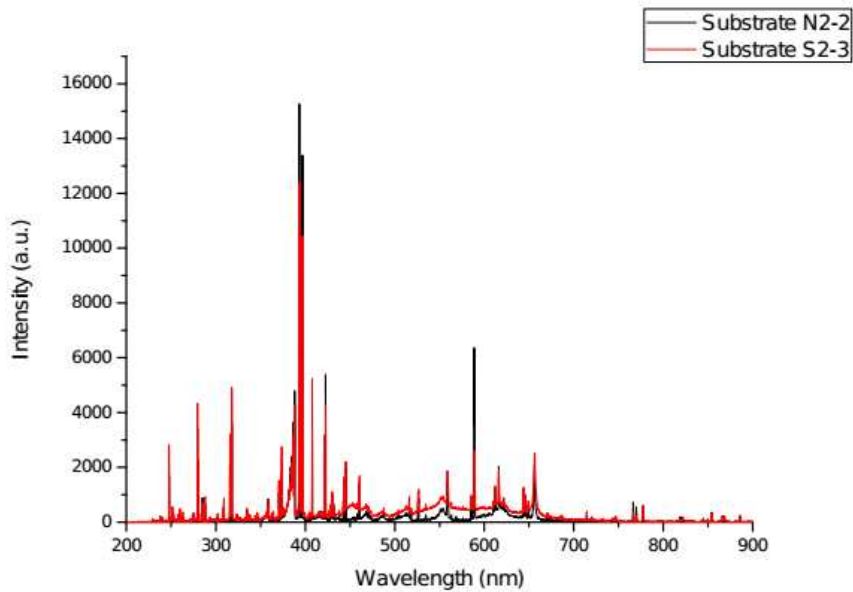
209

Element	Ion.	Wavelength (nm)	$E_k$ ( $\times 10^{-4}$ cm $^{-1}$ )	$A_{ki}$ ( $\times 10^{-8}$ s $^{-1}$ )	$g_k$
Al	I	237.31	4.22	0.81	6
Fe	II	238.20	4.2	3.8	12
Fe	II	239.56	4.21	2.5	10
Fe	II	239.92	4.23	1.4	6
C	I	247.85	6.2	0.18	3
Si	I	250.69	4.0	0.47	5
Si	I	251.61	4.0	1.21	5
Si	I	251.92	3.98	0.46	3
Si	I	252.41	3.97	1.82	1
Si	I	252.85	3.98	0.77	3
Fe	II	258.58	3.87	0.81	8

Fe	II	259.94	3.85	2.2	10
Fe	II	260.65	7.46	1.8	6
Mg	I	285.21	3.51	4.91	3
Si	I	288.15	4.1	1.89	3
Al	I	308.21	3.24	0.63	4
Al	I	309.27	3.24	0.74	6
Ca	II	315.88	5.68	3.1	4
Ca	II	317.93	5.69	3.6	6
Ti	II	336.12	3.0	1.1	10
Ti	II	337.28	2.97	1.11	8
Sr	II	346.44	5.34	2.84	6
Ca	II	370.60	5.22	0.88	2
Ca	II	373.69	5.22	1.7	2
Fe	I	385.99	2.59	0.1	9
Sr	II	407.77	2.45	1.47	4
Sr	II	421.55	2.37	1.34	2
Ca	I	422.67	2.37	2.18	3
Ca	I	442.54	3.77	0.5	3
Ti	I	498.17	2.69	0.66	13
Ti	I	499.10	2.68	0.54	11
Ti	I	499.95	2.67	0.53	9
Ti	I	500.72	2.66	0.49	7

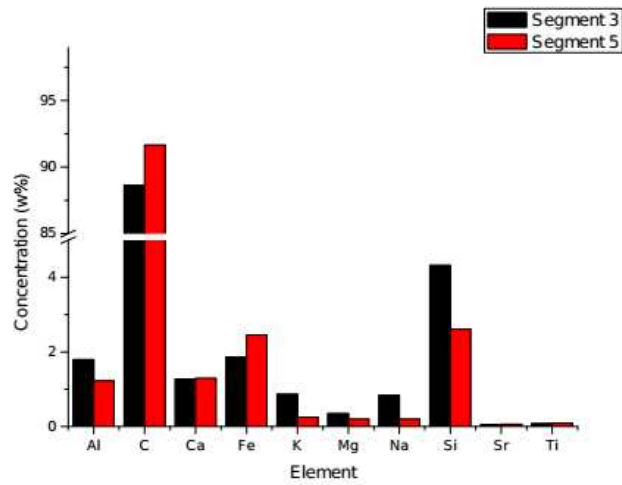
210

211 The analysis evidences that the LIBS spectra of the epoxy resin (segment 3 in sample N2-2 and  
 212 segment 5 in sample S2-3) are very similar in the two samples, and the corresponding elemental  
 213 composition obtained by the CF-LIBS analysis is very similar, as well (figures 7 and 8)



214

215 Figure 7 – Average LIBS spectra of the epoxy resin in samples N2-2 and S2-3



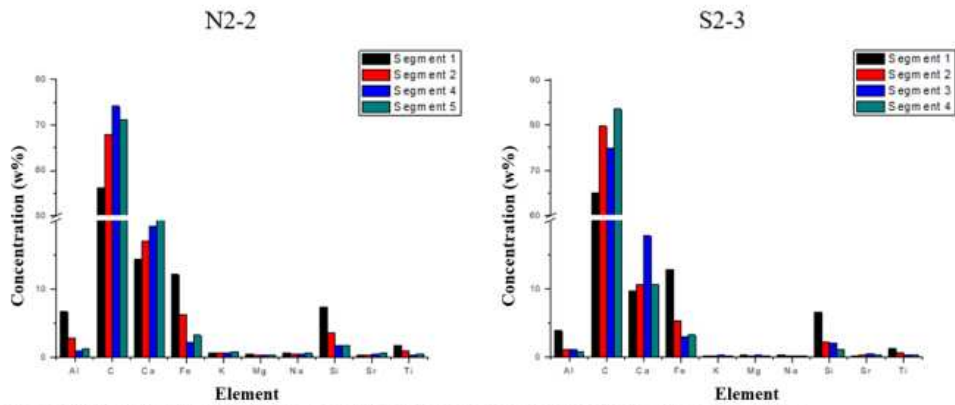
216

217 Figure 8 – Composition of the epoxy resin as determined by CF-LIBS in samples N2-2 (segment 3)  
 218 (segment 5)

219

220 The composition of the other clusters is shown in figure 9, for the two mortar samples.

221



222

223 Figure 9. Results of CF-LIBS obtained for each segmented area (excluding the epoxy resin).

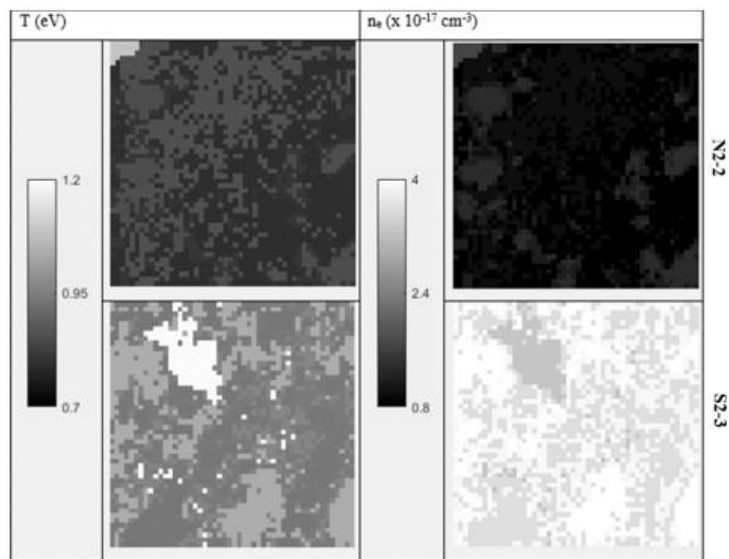
224

225 Although the method presented is independent on the specific instrument used for the acquisition of  
 226 the LIBS spectra, is worth to stress that, in our case, the LIBS spectra were acquired using a time-  
 227 integrated spectrometer. Since the CF-LIBS method relies on the fundamental hypothesis of having  
 228 the plasma close to Local Thermal Equilibrium [43], and this condition occurs in LIBS plasma only  
 229 in a limited time interval, it might seem inappropriate its application to spectra which were acquired  
 230 during the whole lifetime of the plasma. However, the authors have recently demonstrated that, due

231 to the fast decay of the LIBS signal in time, the acquired spectra are in fact dominated by the emission  
232 of the plasma in a time window of about 1  $\mu\text{s}$  [44]. In the time interval considered, typically the LIBS  
233 plasmas are close to LTE conditions, and this consideration gives us confidence that the results  
234 obtained are, indeed, meaningful.

235 The calculate electron temperature and number density are shown on top of the compositional map,  
236 in [figure 10](#). We see that the parts of the map where the epoxy resin was exposed are characterized  
237 by hotter plasmas. This is a further occasion to note that whatever analytical method, applied to the  
238 whole map, would have probably suffered the large differences in the matrix that characterize our  
239 samples.

240



241

242 Figure 10 – Electron temperature and number density as calculated by CF-LIBS

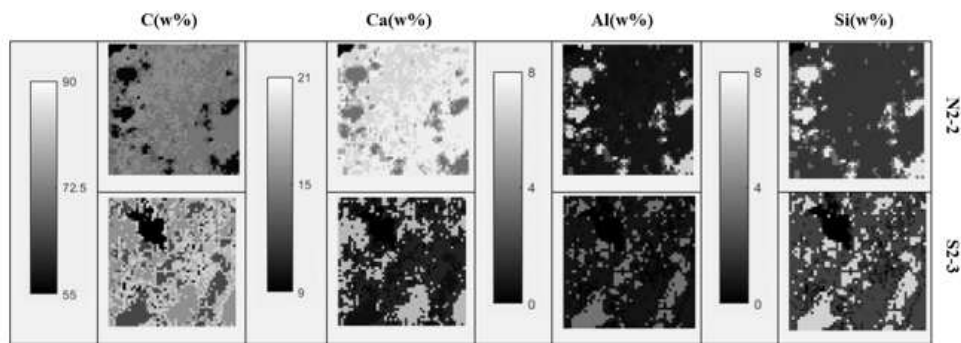
243

244 From the data reported in [figure 9](#), the quantitative compositional maps of the mortars can be obtained.

245 The most significant are shown in figure 11 (the epoxy resin was not considered).

246





247

248 Figure 11 – Quantitative compositional maps of the two mortar samples (top: N2-2, bottom: S2-3)

249

250 The inspection of **figure 11 shows** that the method proposed in this paper, although not able to assess  
 251 the fine compositional variations inside the different groups, provides results that reproduce well the  
 252 texture of the samples. The comparison of the compositional maps obtained confirms quantitatively  
 253 the differences between the two mortars that were already qualitatively evident from the visual  
 254 inspection. **The composition of the constituents of the sample can be obtained with a reasonable**  
 255 **precision, typical of CF-LIBS analysis [45], of about  $\pm 1\%$  on the major elements and proportionally**  
 256 **higher on the minor and trace elements, as evidenced in figure 8, where the same material (epoxy**  
 257 **resin) was analysed in the two samples.** We would like to stress once again that the high  
 258 inhomogeneity of the samples would have made difficult any other quantitative approach based on  
 259 global averages or comparison with reference samples. The CF-LIBS analysis has evidenced, in fact,  
 260 large variations in the plasma parameters (electron temperature and number density, **figure 10**) within  
 261 the same sample and between the two samples that can only be efficiently dealt with using a  
 262 Calibration-Free approach.

263

#### 264 4. Conclusions

265 We have proposed a fast method for the quantitative analysis of  $\mu$ -LIBS elemental images, based on  
 266 the application of the SOM method for the determination of the different classes of materials in the  
 267 samples, followed by CF-LIBS analysis of the average representative spectra.

268 In this way, large variation of the sample matrix can be dealt with, and the textural features of the  
 269 material can be obtained. The technique proposed is transportable, rapid and cheap. It has been  
 270 presented and tested for the realization of compositional maps of historical mortar samples, but it  
 271 could be easily applied to in situ analysis on modern building materials as well as, in general, to the  
 272 analysis of highly inhomogeneous materials.

273

274 **Acknowledgment**

275 This work has been partially supported by MIUR (PRIN 2015 - 2015WBEP3H).

276

277

278 **References**

279

280 [1] J. Koch, D. Günther, Laser Ablation ICP-MS, in: F. Adams, S. Aime, L.A. Andersson, I. Ando,  
281 D.M. Andrenyak, D.L. Andrews, L. Andrews, S.R. Anthony, T.G. Appleton, C.M. Arroyo (Eds.),  
282 Encyclopedia of Spectroscopy and Spectrometry, Elsevier, 2010, pp. 1262-1269.

283

284 [2] A. Riedo, V. Grimaudo, P. Moreno-García, M.B. Neuland, M. Tulej, P. Broekmann, P. Wurz,  
285 Laser ablation/ionisation mass spectrometry: Sensitive and quantitative chemical depth profiling of  
286 solid materials, *Chimia*, (2016), 70 (4), 268-273.

287

288 [3] P.K. Diwakar, J.J. Gonzalez, S.S. Harilal, R.E. Russo, A. Hassanein, Ultrafast laser ablation ICP-  
289 MS: Role of spot size, laser fluence, and repetition rate in signal intensity and elemental fractionation,  
290 *Journal of Analytical Atomic Spectrometry*, (2014), 29 (2), pp. 339-346.

291

292 [4] L. Wang, L.Q. Yang, Y. P. Wang, L. Feng, X. Chen, Z.S. Chen, Developments of laser ablation  
293 inductively coupled plasma mass spectrometry (LA-ICP-MS) in microanalysis, *Geological Bulletin*  
294 *of China*, (2012), 31 (4), pp. 637-645.

295

296 [5] R. Uerlings, A. Matusch, R. Weiskirchen, Reconstruction of laser ablation inductively coupled  
297 plasma mass spectrometry (LA-ICP-MS) spatial distribution images in Microsoft Excel 2007,  
298 *International Journal of Mass Spectrometry*, (2016), 395, pp. 27-35.

299

300 [6] M.L. Warburton, M.R. Reid, C.H. Stirling, G. Closs, Validation of depth-profiling la-ICP-MS in  
301 otolith applications, *Canadian Journal of Fisheries and Aquatic Sciences*, (2017), 74 (4), pp. 572-581.

302

303 [7] K.E. Sjästad, S.L. Simonsen, T. Andersen, Studies of SRM NIST glasses by laser ablation  
304 multicollector inductively coupled plasma source mass spectrometry (LA-ICP-MS), *Journal of*  
305 *Analytical Atomic Spectrometry*, (2012), 27 (6), pp. 989-999.

306

307 [8] O.T. Butler, W.R.L. Cairns, J.M. Cook, C.M. Davidson, Atomic spectrometry update-a review of  
308 advances in environmental analysis, *Journal of Analytical Atomic Spectrometry*, (2017), 32 (1), pp.  
309 11-57.

310

311 [9] Z. Qin, J.A. Caruso, B. Lai, A. Matusch, J.S. Becker, Trace metal imaging with high spatial  
312 resolution: Applications in biomedicine, *Metallomics*, (2011) 3 (1), pp. 28-37.

313

314 [10] P.J. Sylvester, LA-(MC)-ICP-MS trends in 2006 and 2007 with particular emphasis on  
315 measurement uncertainties, *Geostandards and Geoanalytical Research*, (2008) 32 (4), pp. 469-488.

316

317 [11] J.S. Becker, M. Zoriy, B. Wu, A. Matusch, J.S. Becker, Imaging of essential and toxic elements  
318 in biological tissues by LA-ICP-MS, *Journal of Analytical Atomic Spectrometry*, (2008) 23 (9), pp.  
319 1275-1280.

320

321 [12] M.F. La Russa, C.M. Belfiore, V. Comite, D. Barca, A. Bonazza, S.A. Ruffolo, G.M. Crisci, A.  
322 Pezzino, Geochemical study of black crusts as a diagnostic tool in cultural heritage, *Applied Physics*  
323 *A*, (2013) 113 (4), pp. 1151-1162.

324



- 325 [13] B. Giussani, D. Monticelli, L. Rampazzi, Role of laser ablation-inductively coupled plasma-mass  
326 spectrometry in cultural heritage research: A review, *Analytica Chimica Acta*, (2009) 635 (1), pp. 6-  
327 21.
- 328
- 329 [14] J. Almirall, E. Cahoon, S. Jantzi, E. Schenk, T. Trejos, New developments in forensic  
330 applications of LIBS and LA-ICP-MS, *Laser Applications to Chemical, Security and Environmental*  
331 *Analysis*, (2012), LACSEA 2012
- 332
- 333 [15] J. Kaiser, M. Galiová, K. Novotný, R. Červenka, L. Reale, J. Novotný, M. Liška, O. Samek, V.  
334 Kanický, A. Hrdlička, K. Stejskal, V. Adam, R. Kizek, Mapping of lead, magnesium and copper  
335 accumulation in plant tissues by laser-induced breakdown spectroscopy and laser-ablation inductively  
336 coupled plasma mass spectrometry, *Spectrochimica Acta B*, (2009) 64 (1), pp. 67-73.
- 337
- 338 [16] B.T. Manard, C. Derrick Quarles, E.M. Wylie, N. Xu, Laser ablation-inductively couple plasma-  
339 mass spectrometry/laser induced break down spectroscopy: A tandem technique for uranium particle  
340 characterization, *Journal of Analytical Atomic Spectrometry*, (2017) 32 (9), pp. 1680-1687
- 341
- 342 [17] L. Sancey, V. Motto-Ros, B. Busser, S. Kotb, J.M. Benoit, A. Piednoir, F. Lux, O. Tillement, G.  
343 Panczer, J. Yu, Laser spectrometry for multi-elemental imaging of biological tissues *Scientific*  
344 *Reports*, (2014) 4, art. no. 6065
- 345
- 346 [18] L. Krajcarová, K. Novotný, M. Kummerová, J. Dubová, V. Gloser, J. Kaiser, Mapping of the  
347 spatial distribution of silver nanoparticles in root tissues of *Vicia faba* by laser-induced breakdown  
348 spectroscopy (LIBS)(2017) *Talanta*, 173, pp. 28-35
- 349
- 350 [19] N. Hausmann, P. Siozos, A. Lemonis, A.C. Colonese, H.K. Robson, D. Anglos, Elemental  
351 mapping of Mg/Ca intensity ratios in marine mollusc shells using laser-induced breakdown  
352 spectroscopy, *Journal of Analytical Atomic Spectrometry*, (2017) 32 (8), pp. 1467-1472.
- 353
- 354 [20] P. Fichet, J. Lacour, D. Menut, P. Mauchien, A. Rivoallan, C. Fabre, J. Dubessy, M.C. Boiron,  
355 micro LIBS technique, in: *Laser-Induced Breakdown Spectroscopy: Principles and Applications*,  
356 A.Miziolek, V.Palleschi and I.Schechter (eds.), Cambridge University Press ,2006, pp. 539-555.
- 357
- 358 [21] H. Bette, R. Noll, Laser induced breakdown spectroscopy at 1000 Hz with single pulse for high-  
359 speed, high-resolution chemical element mapping, *Conference on Lasers and Electro-Optics Europe*  
360 *- Technical Digest*, (2003), art. no. 1313540, 477
- 361
- 362 [22] K. Novotný, J. Kaiser, M. Galiová, V. Konečná, J. Novotný, R. Malina, M. Liška, V. Kanický,  
363 V. Otruba, Mapping of different structures on large area of granite sample using laser-ablation based  
364 analytical techniques, an exploratory study, *Spectrochimica Acta B*, (2008) 63 (10), pp. 1139-1144.
- 365
- 366 [23] C. Schiavo, L. Menichetti, E. Grifoni, S. Legnaioli, G. Lorenzetti, F. Poggialini, S. Pagnotta,  
367 V. Palleschi, High-resolution three-dimensional compositional imaging by double-pulse laser-  
368 induced breakdown spectroscopy *Journal of Instrumentation*, (2016) 11 (8), art. no. C08002
- 369
- 370 [24] R. Grassi, E. Grifoni, S. Gufoni, S. Legnaioli, G. Lorenzetti, N. Macro, L. Menichetti, S.  
371 Pagnotta, F. Poggialini, C. Schiavo, V. Palleschi, Three-dimensional compositional mapping using



- 372 double-pulse micro-laser-induced breakdown spectroscopy technique, *Spectrochimica Acta B*,  
373 (2017) 127, pp. 1-6  
374
- 375 [25] E. Tognoni, G. Cristoforetti, S. Legnaioli, V. Palleschi, Calibration-Free Laser-Induced  
376 Breakdown Spectroscopy: State of the art, *Spectrochimica Acta B*, (2010) 65 (1), pp. 1-14  
377
- 378 [26] A. Ciucci, M. Corsi, V. Palleschi, S. Rastelli, A. Salvetti, E. Tognoni., New procedure for  
379 quantitative elemental analysis by laser-induced plasma spectroscopy, *Applied Spectroscopy*, (1999)  
380 53 (8), pp. 960-964  
381
- 382 [27] T. Takahashi, B. Thornton, Quantitative methods for compensation of matrix effects and self-  
383 absorption in LIBS signals of solids, *Spectrochimica Acta B*, (2017) 138, pp. 31-42  
384
- 385 [28] E. D'Andrea, S. Pagnotta, E. Grifoni, S. Legnaioli, G. Lorenzetti, V. Palleschi, B. Lazzerini, A  
386 hybrid calibration-free/artificial neural networks approach to the quantitative analysis of LIBS  
387 spectra, *Applied Physics B*, (2015) 118 (3), pp. 353-360.  
388
- 389 [29] S. Pagnotta, M. Lezzerini, L. Ripoll-Seguer, M. Hidalgo, E. Grifoni, S. Legnaioli, G. Lorenzetti,  
390 F. Poggialini, V. Palleschi, Micro-Laser-Induced Breakdown Spectroscopy (Micro-LIBS) Study on  
391 Ancient Roman Mortars, *Applied Spectroscopy*, (2017) 71 (4), pp. 721-727  
392
- 393 [30] F. Massazza, Pozzolana and pozzolanic cements, *Lea's Chemistry of Cement and Concrete*,  
394 (2003), pp. 471-635  
395
- 396 [31] J. Válek, J.J. Hughes, C.J.W.P. Groot, Historic mortars: Characterisation, assessment and repair.  
397 A state-of-the-art summary, *RILEM Bookseries*, (2013) 7, pp. 1-12  
398
- 399 [32] M. Lezzerini, M. Ramacciotti, F. Cantini, B. Fatighenti, F. Antonelli, E. Pecchioni, F. Fratini, E.  
400 Cantisani, M. Giamello, Archaeometric study of natural hydraulic mortars: the case of the Late  
401 Roman Villa dell'Oratorio (Florence, Italy), *Archaeol. Anthropol. Sci.*, (2017) 9, pp. 603-615  
402
- 403 [33] G. Gallelo, M. Ramacciotti, M. Lezzerini, E. Hernandez, M. Calvo, A. Morales, A. Pastor, M.  
404 De la Guardia, Indirect chronology method employing rare earth elements to identify Sagunto Castle  
405 mortar construction periods, *Microchemical Journal*, (2017) 132, pp. 251-261.  
406
- 407 [34] N. Li, N. Farzadnia, C. Shi, Microstructural changes in alkali-activated slag mortars induced by  
408 accelerated carbonation, *Cem. Concr. Res.*, (2017) 100, pp. 214-226  
409
- 410 [35] P. Ubbriaco, F. Tasselli, A Study of the Hydration of Lime-Pozzolan Binders, *J. Therm. Anal.*  
411 *Calorim.*, (1998) 52, pp. 1047-1054  
412
- 413 [36] C.M. Belfiore, G.V. Fichera, G. Ortolano, A. Pezzino, R. Visalli, L. Zappalà, Image processing  
414 of the pozzolanic reactions in Roman mortars via X-Ray Map Analyser, *Microchem. J.*, (2016) 125,  
415 pp. 242-253.  
416
- 417 [37] A. Bertolini, G. Carelli, F. Francesconi, M. Francesconi, L. Marchesini, P. Marsili, F.  
418 Sorrentino, G. Cristoforetti, S. Legnaioli, V. Palleschi, L. Pardini, A. Salvetti, *Modi: A new mobile*

419 instrument for in situ double-pulse LIBS analysis, *Analytical and Bioanalytical Chemistry*, (2006)  
420 385 (2), pp. 240-247.  
421  
422 [38] P.A. Benedetti, G. Cristoforetti, S. Legnaioli, V. Palleschi, L. Pardini, A. Salvetti, E. Tognoni,  
423 Effect of laser pulse energies in laser induced breakdown spectroscopy in double-pulse configuration,  
424 *Spectrochimica Acta B*, (2005) 60 (11), pp. 1392-1401  
425  
426 [39] T. Kohonen, The self-organizing map, *Neurocomputing*, (1998) 21, pp. 1-6  
427  
428 [40] P.M. Atkinson, A.R.L. Tatnall, Introduction neural networks in remote sensing, *Int. J. Remote*  
429 *Sens.*, (1997) 18, pp. 699-709  
430  
431 [41] T. Villmann, E. Merényi, B. Hammer, Neural maps in remote sensing image analysis *Neural*  
432 *Networks*, (2003) 16, pp. 389-403  
433  
434 [42] I.K. Fodor, A survey of dimension reduction techniques, Lawrence Livermore National Lab.,  
435 CA (US), 2002  
436  
437 [43] G. Cristoforetti, A. De Giacomo, M. Dell'Aglio, S. Legnaioli, E. Tognoni, V. Palleschi, N.  
438 Omenetto, Local Thermodynamic Equilibrium in Laser-Induced Breakdown Spectroscopy: Beyond  
439 the McWhirter criterion, *Spectrochimica Acta B*, (2010) 65 (1), 86-95.  
440  
441 [44] E. Grifoni, S. Legnaioli, M. Lezzerini, G. Lorenzetti, S. Pagnotta, V. Palleschi, Extracting time-  
442 resolved information from time-integrated laser-induced breakdown spectra, *Journal of*  
443 *Spectroscopy*, (2014), art. no. 849310  
444  
445 [45] E. Tognoni, G. Cristoforetti, S. Legnaioli, V. Palleschi, A. Salvetti, M. Mueller, U. Panne, I.  
446 Gornushkin, A numerical study of expected accuracy and precision in Calibration-Free Laser-Induced  
447 Breakdown Spectroscopy in the assumption of ideal analytical plasma, *Spectrochimica Acta B*,  
448 (2007) 62 (12), pp. 1287-1302.  
449  
450  
451